Asymmetry and stability of shape kinematics in microswimmers' motion

Yizhar Or*
Faculty of Mechanical Engineering, Technion - Israel Institute of Technology, Israel

Many swimming microorganisms governed by low-Reynolds-Number hydrodynamics utilize flagellar undulations for self propulsion. Most of existing theoretical models assume that the shape kinematics is directly controlled, while in reality, eukaryotes actuate internal bending moments along their flagellum. Under this control, the shape is dynamically evolving and periodic gaits may become unstable. The paper addresses this problem by revisiting Purcell's three-link swimmer model where joint torques are controlled, and the geometric symmetries underlying the dynamics of the swimmer are analyzed. It is found that one has to break the front-back symmetry of the swimmer's structure and/or actuation profile in order to induce stable shape kinematics. The results may explain why most of the flagellated eukaryotes swim with their head forward.

The motion of swimming microorganisms is governed by low Reynolds Number (Re) hydrodynamics, where viscous effects dominate and inertial effects are negligible [1]. Eukaryotic cells use undulations of their flagella in order to generate net motion [2], and engineers are striving to mimic this success in designing artificial nano-robotic swimmers, primarily intended for biomedical applications [3]. Theoretical analysis of low-Re locomotion is a highly active research area, cf. [4], where a classical example is the three-link swimmer model proposed by Purcell [5], which was further analyzed in [6]. All these works have made the simplifying assumption that the swimmer directly controls the kinematics of its changing shape. However, in reality, swimming microorganisms such as eukaryotic cells typically prescribe a time-varying distribution of bending moments along their flagellum, generated by molecular motors [7, 8]. The shape kinematics, as well as swimming motion, are then evolving dynamically as a result of interaction between the controlled actuation, material elasticity, and viscous drag [9]. Importantly, using the assumption of controlled force/torque actuation instead of controlled shape kinematics poses a problem of *dynamic stability* of the shape kinematics, which do not necessarily converge to a time-periodic gait. In order to address this problem, the paper revisits Purcell's three link swimmer model and analyzes its dynamics under actuation of controlled motor torques at the joints. Since in some scenarios of high viscosity, elastic effects become small compared to viscous drag forces (cf. [10, 11]), elasticity effects are neglected in this model for simplicity. The analysis focuses on dynamic stability of periodic shape kinematics under periodic torque actuation. The geometric symmetries underlying the dynamics are analyzed, and it is shown that one has to maintain an actuation profile which is symmetric with respect to the swimmer's longitudinal axis in order to induce straight-line swimming, and to break the front-back symmetry in the swimmer's structure and/or actuation profile in order to induce dynamically stable shape kinematics. The results are demonstrated in numerical simulations based on resistive force theory. It is found that a swimmer with a stronger torque actuation at its back and/or larger drag resistance at its front possesses stable shape kinematics, where the undulation amplitude increases from head to tail. This may suggest an explanation why most of the flagellated eukaryotes swim with their head forward.

We begin by describing Purcell's three-link swimmer model and formulating the dynamic equations which govern its motion. The swimmer, depicted in Fig. 1(a), consists of three elongated rigid links whose lengths are l_0, l_1 and l_2, which are connected by two rotary joints. Typically, the two distal links are assumed to be identical $l_1 = l_2$, and the swimmer's motion is assumed to be confined to the xy plane. The shape of the swimmer is described by the two relative angles between the links, denoted by $\mathbf{s} = (\phi_1, \phi_2)^T$. The state of the swimmer is described by the planar position and orientation of a reference frame which is attached to the central link, and is denoted by $\mathbf{q} = (x, y, \theta)^T$. The swimmer is actuated by two internal torques τ_1 and τ_2 acting at the rotary joints [Fig. 1(a)]. The controlled input of the swimmer is de-

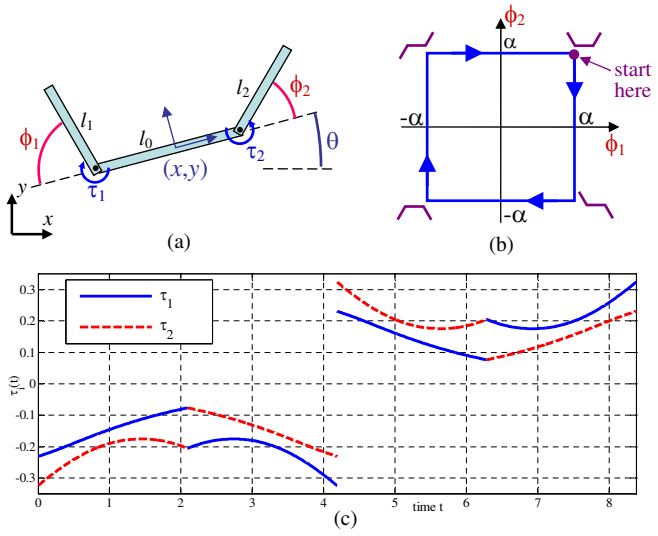

FIG. 1: (a) Purcell's three-link swimmer model. (b) The square gait in (ϕ_1, ϕ_2)-plane. (c) The time profile of joint torques $\tau_i(t)$ under the square gait.

noted by $\boldsymbol{\tau} = (\tau_1, \tau_2)^T$, and it is assumed that a given time-profile of $\boldsymbol{\tau}(t)$ is imposed. The swimmer is submerged in an unbounded domain of viscous fluid whose motion is governed by Stokes equations [1]. The motion of the swimmer depends on the change in its shape, as described by the differential equation

$$\dot{\mathbf{q}} = \mathbf{G}(\mathbf{q}, \mathbf{s})\dot{\mathbf{s}}. \tag{1}$$

Additionally, the shape of the swimmer is governed by the controlled torque input, as described by the differential equation

$$\dot{\mathbf{s}} = \mathbf{H}(\mathbf{s})\boldsymbol{\tau}. \tag{2}$$

The detailed derivation of the equations of motion is given in the supplementary document [18]. It is based on the facts that for rigid bodies in Stokes flow, forces and velocities are linearly related by a resistance tensor [1], and that the motion is quasi-steady, so that each rigid body is in static equilibrium at all times. Moreover, explicit expressions for $\mathbf{G}(\mathbf{q}, \mathbf{s})$ and $\mathbf{H}(\mathbf{s})$ are derived in [18] by utilizing *resistive force theory* (RFT) [12]. It is assumed that the input $\boldsymbol{\tau}(t)$ is T-periodic, i.e. satisfies $\boldsymbol{\tau}(t+T) = \boldsymbol{\tau}(t)$. Importantly, a periodic actuation input $\boldsymbol{\tau}(t)$ does not necessarily imply periodic shape kinematics $\mathbf{s}(t)$. The continuous-time dynamics in (1) and (2) induce the discrete-time dynamics (also known as the Poincaré recurrence map [13]) given by

$$\mathbf{q}_{k+1} = \mathcal{G}(\mathbf{q}_k, \mathbf{s}_k) \text{ and } \mathbf{s}_{k+1} = \mathcal{H}(\mathbf{s}_k), \tag{3}$$

where $\mathbf{q}_k = \mathbf{q}(t = kT)$, $\mathbf{s}_k = \mathbf{s}(t = kT)$ and $k \in \mathbb{N}$. A T-periodic shape change $\mathbf{s}^*(t)$ corresponds to a *fixed point* $\mathbf{s}_e = \mathbf{s}^*(0)$ of the map $\mathcal{H}$ in (3), which satisfies $\mathcal{H}(\mathbf{s}_e) = \mathbf{s}_e$. The following dynamic simulation example illustrates the stability problem of shape kinematics which may arise under the torque-control assumption. Consider the classical square gait of shape changes $\mathbf{s}(t)$ shown in the closed loop in (ϕ_1, ϕ_2)-plane in Fig 1(b), for Purcell's swimmer with identical links, i.e. $l_0 = l_1 = l_2$. This gait was widely studied in [5], and is known to generate straight-line net motion sideways. Using the expressions derived in [18] by RFT formulation, numerical simulation gives the time profile of internal torques $\tau_i(t)$ required to generate this gait, which is shown in Fig. 1(c), for amplitude $\alpha = 60°$ and constant rate $\dot{\phi}_i = 1$. Next, we assume that the same time profile $\boldsymbol{\tau}(t)$ is used as a periodic input but the swimmer starts at a straightened configuration, that is, the initial conditions are $\mathbf{s}(0) = (0°, 0°)^T$, and the equations (1) and (2) are integrated numerically. Fig. 2(a) plots the resulting trajectory of $\mathbf{s}(t)$ in (ϕ_1, ϕ_2)-plane. Obviously, even though the torque input is periodic, the shape trajectory does not follow a closed loop and no periodic gait is generated. That is, the periodic solution $\mathbf{s}(t)$ in Fig. 1(b) is *unstable* with respect to changes in the initial conditions. Fig. 2(b) shows snapshots of the swimmer's

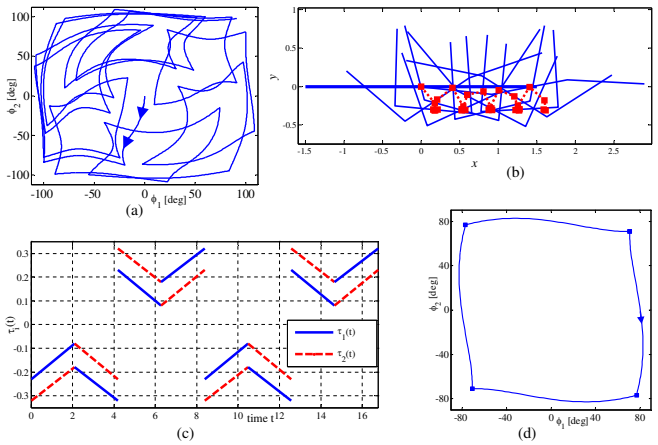

FIG. 2: (a) Trajectories of $\mathbf{s}(t)$ in (ϕ_1, ϕ_2)-plane for $\mathbf{s}(0) = (0, 0)^T$. (b) Snapshots of the swimmer at times $t = 3kT$ (c) Linear time profile of joint torques $\tau_i(t)$. (d) The periodic orbit in (ϕ_1, ϕ_2)-plane under the linear time profile of $\boldsymbol{\tau}(t)$.

state and shape at times $t = 3kT$, i.e. every three cycles, where the thick line is the initial straightened configuration. Additionally, the centerpoint of the middle link at times $t = kT$ is marked by squares connected by dashed lines. Clearly, the trajectory of the swimmer's net motion does not follow a straight line path as desired, and resembles a chaotic-like tumble. This example motivates the following three key questions: First, how can one choose a time profile for the torque input $\boldsymbol{\tau}(t)$ which will result in periodic shape change $\mathbf{s}(t)$? Second, how can one choose periodic input $\boldsymbol{\tau}(t)$ which will result in net motion of the swimmer along a straight line? Third, is it possible to induce a periodic shape change $\mathbf{s}(t)$ which will be *asymptotically stable* under changes in the initial conditions?

In order to address these questions, one needs to study symmetries in the geometric structure of the swimmer. The swimmer possesses two reflection symmetries: one about the longitudinal axis of the central link – *axisymmetry*, and one about the line perpendicular to it – *front-back symmetry*, which holds only when the two distal links are identical $l_1 = l_2$. This implies symmetries on $\mathbf{G}(\mathbf{q}, \mathbf{s})$ and $\mathbf{H}(\mathbf{s})$ in (1) and (2), which are detailed in [18]. Based on these symmetries, two time-symmetry properties of the control input are defined as follows. A T-periodic control input $\boldsymbol{\tau}(t)$ is called *reversible* if it satisfies $\boldsymbol{\tau}(T - t) = -\mathbf{M}_s\boldsymbol{\tau}(t)$ where $\mathbf{M}_s = \begin{pmatrix} 0 & 1 \\ 1 & 0 \end{pmatrix}$, and is called *axisymmetric* if it satisfies $\boldsymbol{\tau}(t + T/2) = -\boldsymbol{\tau}(t)$ for all t. Note that the control input $\boldsymbol{\tau}(t)$ in Fig. 1(c), which is associated with the square gait $\mathbf{s}(t)$ in Fig. 1(b), is both reversible and axisymmetric. The following four key results, whose proofs are detailed in [18], utilize the two properties of $\boldsymbol{\tau}(t)$ defined above in order to guarantee existence of time-periodic solution of shape kinematics, and to generate straight-line net motion:

Result 1: For a front-back symmetric swimmer, i.e. $l_1 = l_2$, if $\boldsymbol{\tau}(t)$ is a reversible input and under initial condition $\mathbf{s}(0) = (\alpha, \alpha)^T$ the solution of (2) satisfies $\mathbf{s}(T/2) = (\beta, \beta)^T$ for some α, β, then $\mathbf{s}(t)$ is T-periodic.
Result 2: If $\boldsymbol{\tau}(t)$ is an axisymmetric input and the solution of (2) satisfies $\mathbf{s}(T/2) = -\mathbf{s}(0)$, then $\mathbf{s}(t)$ is T-periodic and satisfies $\mathbf{s}(t + T/2) = -\mathbf{s}(t)$. Moreover, the solution of $\mathbf{q}(t)$ in (1) satisfies $\theta(T) = \theta(0)$. That is, the control input induces a periodic gait which results in net motion of pure translation and zero rotation. Importantly, note that this result holds also for $l_1 \neq l_2$.
Result 3: For a front-back symmetric swimmer, i.e. $l_1 = l_2$, if the control input $\boldsymbol{\tau}(t)$ is both reversible and axisymmetric and under initial condition $\mathbf{s}(0) = (\alpha, \alpha)^T$, the solution of (2) satisfies $\mathbf{s}(T/4) = (\beta, -\beta)^T$ for some α, β, then $\mathbf{s}(t)$ is T-periodic and satisfies $\mathbf{s}(T/2) = (-\alpha, -\alpha)^T$ and $\mathbf{s}(3T/4) = (-\beta, \beta)^T$. Moreover, the solution of (1) satisfies $\theta(T) = \theta(0)$ and $y(T) = y(0)$. (That is, straight-line net motion along x-direction).

These results can be utilized for constructing a time profile of a control input $\boldsymbol{\tau}(t)$ which results in periodic shape change that induces straight-line motion. For example, one can start with an arbitrary time profile for $\boldsymbol{\tau}(t)$ from initial condition $\mathbf{s}(0) = (\alpha, \alpha)^T$, and proceed until a time t_c at which the solution $\mathbf{s}(t)$ hits the line $\phi_1 = -\phi_2$. Then, a reversible and axisymmetric T-periodic input with $T = 4t_c$ can be constructed by continuation of $\boldsymbol{\tau}(t)$ according to the symmetry rules $\boldsymbol{\tau}(t_c + t) = \mathbf{M}_s \boldsymbol{\tau}(t_c - t)$ and $\boldsymbol{\tau}(2t_c + t) = -\boldsymbol{\tau}(t)$. Alternatively, one can construct an arbitrary reversible and axisymmetric input and then numerically search for its corresponding periodic solution $\mathbf{s}(t)$. For example, the control input shown in Fig. 2(c) is a linear approximation of the one obtained in Fig. 1(c) for the square gait. Numerical search leads to the periodic solution $\mathbf{s}^*(t)$ which is the closed loop in (ϕ_1, ϕ_2)-plane shown in Fig. 2(d). A plot of motion snapshots of the swimmer's state and shape during a complete period is given in [18], which shows that the net motion of the swimmer is indeed pure translation along the x direction.

In order to study the asymptotic convergence of the shape trajectory $\mathbf{s}(t)$ to the periodic solution $\mathbf{s}^*(t)$ under changes in the initial condition, one has to investigate its dynamic stability. A fundamental fact in dynamical systems theory [13] is that the local (i.e. under small perturbations) stability of the periodic solution is equivalent to the local stability of the fixed point $\mathbf{s}_e = \mathbf{s}^*(0)$ of the Poincaré recurrence map $\mathcal{H}(\cdot)$ in (3). This stability, in turn, is determined by the eigenvalues of the Jacobian matrix $\left[\frac{\partial \mathcal{H}}{\partial \mathbf{s}}(\mathbf{s}=\mathbf{s}_e)\right]$. If all eigenvalues lie within the unit disc in the complex plane (i.e. have magnitude less than one) then $\mathbf{s}_e$ and the corresponding periodic solution $\mathbf{s}^*(t)$ are locally asymptotically stable. If one eigenvalue or more lie strictly outside the unit disc, then $\mathbf{s}_e$ and $\mathbf{s}^*(t)$ are unstable. We now invoke another key fact which stems from the symmetry properties of (1),(2) and from the definition of a reversible input.
Result 4: For a front-back symmetric swimmer, i.e. $l_1 = l_2$, if $\boldsymbol{\tau}(t)$ is reversible, then the map $\mathcal{H}$ satisfies

$$\mathcal{H}(\mathbf{M}_s \mathbf{s}) = \mathbf{M}_s \mathcal{H}^{-1}(\mathbf{s}) \text{ where } \mathbf{M}_s = \begin{pmatrix} 0 & 1 \\ 1 & 0 \end{pmatrix}. \quad (4)$$

The relation (4) is called a *reversing symmetry* of the map $\mathcal{H}$ [14]. Next, we note that according to Result 1, a reversible input $\boldsymbol{\tau}(t)$, induces a periodic solution $\mathbf{s}^*(t)$ such that $\mathbf{s}^*(0) = \mathbf{s}_e = (\alpha, \alpha)$ is a fixed point of the map $\mathcal{H}$. Such a point is called a *reversible equilibrium*, since it lies in the fixed set of the reversing symmetry, i.e., it satisfies $\mathbf{M}_s \mathbf{s}_e = \mathbf{s}_e$. This fact leads to the next key result which characterizes the linearization eigenvalues of a reversible equilibrium of a map.
Result 5 ([14]): If λ is an eigenvalue of the linearization about a reversible equilibrium of a map, then so are $1/\lambda$ and $\bar{\lambda}$.
Since the map $\mathcal{H}$ in (3) is of dimension two, the linearization has two eigenvalues which must satisfy $\lambda_2 = 1/\lambda_1 = \bar{\lambda}_1$. In case where the eigenvalues are real, $\lambda_1 = r$, $\lambda_2 = 1/r$ for some $r \in I\!R$, then generically one of them lies outside of the unit disc, hence the equilibrium point is unstable. In case where the two eigenvalues are complex, they must lie on the unit circle and take the form $\lambda_{1,2} = e^{\pm i\omega}$. Then, according to a known result [14], the reversible equilibrium $\mathbf{s}_e$ possesses *marginal stability*, that is, under small perturbations the deviation $\mathbf{s}(t) - \mathbf{s}^*(t)$ remains bounded but does not tend asymptotically to zero.

So far we have shown that the reversing symmetry implies marginal stability. Now we proceed to show how breaking the symmetry results in asymptotic stability. A key fact is that under a continuous change in $\mathbf{H}(\mathbf{s})$ and $\boldsymbol{\tau}(t)$, the solution of (2) changes continuously. This induces a continuous change of the map $\mathcal{H}$ in (3), which generically results in a continuous change in its fixed point $\mathbf{s}_e$. Thus, the eigenvalues of the linearization about $\mathbf{s}_e$ also change continuously. If under reversing symmetry the two eigenvalues lie on the unit circle, they will generically shift either inside or outside the unit circle. If they shift strictly inside the unit circle, then the new equilibrium point is asymptotically stable. If they shift outside the unit circle, then the new equilibrium point is unstable. Nevertheless, if the control input is now played in reverse time, i.e. $\boldsymbol{\tau}(t) \to -\boldsymbol{\tau}(-t)$, the maps in (3) are inverted $\mathcal{H} \to \mathcal{H}^{-1}$, $\mathcal{G} \to \mathcal{G}^{-1}$. The fixed point $\mathbf{s}_e$ is preserved, but the linearization eigenvalues are inverted $\lambda_i \to 1/\lambda_i$, and now lie inside the unit circle, implying asymptotic stability of $\mathbf{s}_e$ in reversed time. Therefore, when the reversing symmetry is broken, the swimmer has a *preferred direction* in which the periodic gait $\mathbf{s}(t)$ becomes asymptotically stable. Importantly, this stability is a purely passive effect (or open-loop) and does not

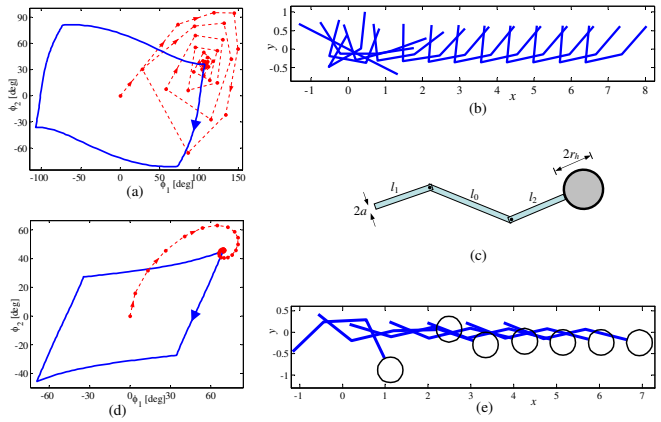

FIG. 3: (a) Points of $\mathbf{s}(t=kT)$ in (ϕ_1,ϕ_2)-plane for $\mathbf{s}(0)=(0,0)^T$ (dots) and the periodic solution $\mathbf{s}^*(t)$ (solid curve) for $\kappa=1.25$. (b) Snapshots of the swimmer at times $t=4kT$ for $\kappa=1.25$. (c) The three link swimmer with a spherical head. (d) Points of $\mathbf{s}(t=kT)$ in (ϕ_1,ϕ_2)-plane for $\mathbf{s}(0)=(0,0)^T$ (dots) and the periodic solution $\mathbf{s}^*(t)$ (solid curve) for the swimmer with head. (e) Snapshots at times $t=T/4+8kT$ for the swimmer with head.

involve any feedback using measurement of swimmer's position or joint angles in real time.

Two ways for breaking the reversing symmetry are possible: the first way is changing the control input $\boldsymbol{\tau}(t)$ in a way that violates the reversibility property of the actuation; the second is changing the structure of the swimmer in a way that breaks its front-back symmetry. In order to demonstrate this stability result in simulations, we consider the linear control input $\boldsymbol{\tau}(t)$ shown in Fig. 2(c), which results in a marginally stable periodic orbit $\mathbf{s}^*(t)$ shown in Fig. 2(d), and break the symmetry in the two ways described above. First, we modify the input $\boldsymbol{\tau}(t)$ by multiplying $\tau_1(t)$ by a scalar κ while $\tau_2(t)$ is multiplied by $1/\kappa$. This changes the relative strengths of the actuation at the two joints, so that the reversibility property of $\boldsymbol{\tau}(t)$ is violated, while it still remains axisymmetric. For value of $\kappa=1.25$, numerical simulation give the equilibrium point $\mathbf{s}_e=(107.4^\circ,36.2^\circ)^T$ and linearization eigenvalues of $\lambda_{1,2}=0.86e^{\pm 1.84i}$, implying asymptotic stability. Next, numerical simulation was conducted for initial conditions $\mathbf{s}(0)=(0,0)^T$ under the asymmetric input. The once-per-cycle values $\mathbf{s}(kT)$ are shown as dots connected by dashed lines in Fig. 3(a), and the solid closed curve is the steady-state periodic trajectory $\mathbf{s}^*(t)$. (Showing the full trajectory of $\mathbf{s}(t)$ would make the plot too dense). The plot shows asymptotic convergence of the shape changes $\mathbf{s}(t)$ to the periodic orbit $\mathbf{s}^*(t)$. Fig. 3(b) shows snapshots of the swimmer at times $t=4kT$, i.e. every four cycles. It can be seen that the swimmer rapidly converges to the steady periodic motion and also travels along a straight line without net rotation. This is in accordance with result 2, since the non-reversible input $\boldsymbol{\tau}(t)$ is still axisymmetric.

In the second example of symmetry breaking, we keep the same reversible control input $\boldsymbol{\tau}(t)$ shown in Fig. 2(c), and break the front-back symmetry of the swimmer's structure by adding a spherical 'head' of radius r_h at the end of the right link [Fig. 3(c)] in order to mimic the structure of a flagellated eukaryotic cell. The details on how to formulate approximate equations of motion in this case by neglecting hydrodynamic interactions are given in [18]. We simulated a swimmer where the three links have length 1 and radius 0.1 while the spherical head has radius 0.3. Again, Fig. 3(d) shows the once-per-cycle points $\mathbf{s}(kT)$ as dots connected by dotted lines, and the periodic solution $\mathbf{s}^*(t)$ as a closed curve in (ϕ_1,ϕ_2)-plane. Fig. 3(e) shows snapshots of the swimmer at times $t=\frac{1}{4}T+8kT$, demonstrating convergence to the periodic motion. An observation from the shapes of the periodic solutions $\mathbf{s}^*(t)$ in Fig. 3(a) and 3(d) is that in both cases the amplitude of ϕ_1 is notably greater than that of ϕ_2. That is, stable swimming produces undulations where the *amplitude is increasing from head to tail*. This is in agreement with observations on the waveform of sperm cells in motion [7, 10]. Note that this asymmetry can be achieved either by placing stronger actuation at the back ($|\tau_2|>|\tau_1|$) of a front-back symmetric swimmer, or by symmetric actuation for a swimmer with a front link that experiences larger drag resistance (spherical head vs. slender tail).

In summary, the paper has analyzed the dynamics of Purcell's three-link microswimmer under controlled torque actuation. It has been shown that in the front-back symmetric case, the periodic shape kinematics is a marginally stable solution, and that breaking the symmetry in the swimmer's structure and/or actuation profile induces a preferred swimming direction for which the shape kinematics becomes asymptotically stable. This is another example on how symmetry-breaking implies dynamic stability in low-*Re* locomotion dynamics, in addition to previous studies on swimmer's attraction to a wall [15] and on phase synchronization of two flagellated microorganisms [16]. It is important to note that the stability results presented here rely on symmetries which are consequence of the geometric structure of the swimmer, and do not depend on the detailed hydrodynamic model. That is, the results should also hold if a more accurate model of the hydrodynamic interactions is used instead of resistive force theory.

We now briefly list some open problems for future research. First, the numerical simulation results should be augmented by analytical arguments and parametric analysis based on asymptotic methods. Second, extending the theoretical model in order to account for the effects of hydrodynamic interaction and to consider continuous elastic filaments in the spirit of [9], or its discretization as a multiple-link chain are challenging theoretical problems. As a preliminary step, the motion of Purcell's three-link swimmer with one actuated joint and a passive

elastic joint has been recently analyzed in [17]. Third, considering the torque-actuated swimmer model near a no-slip wall will result in a more complicated dynamical system which combines the effects studied here with those in [15]. Finally, a macro scale three-link robotic swimmer for experimental demonstration of the results is currently under development (see picture in [18]).

* izi@tx.technion.ac.il

[1] J. Happel and H. Brenner, *Low Reynolds Number Hydrodynamics* (Prentice-Hall, 1965).

[2] T. J. Pedley and J. O. Kessler, Annu. Rev. Fluid Mech. **24**, 313 (1992); E. Lauga and T. R. Powers, Rep. Prog. Phys. **72**, 096601 (2009).

[3] R. Dreyfus, J. Baudry, M. l. Roper, M. Fermigier, H. A. Stone, and J. Bibette, Nature **437**, 862 (2005); B. J. Nelson, I. K. Kaliakatsos, and J. J. Abbott, Review of Biomedical Engineering **12**, 55 (2010).

[4] G. I. Taylor., Proc. Roy. Soc. A **209**, 447 (1951); H. A. Stone and A. D. T. Samuel, Physical Review Letters **77**, 4102 (1996); A. Najafi and R. Golestanian, Phys. Rev. E **69**, 062901 (2004).

[5] E. M. Purcell, Am. J. Phys. **45**, 3 (1977); L. E. Becker, S. A. Koehler, and H. A. Stone, J. Fluid Mech. **490**, 15 (2003).

[6] D. Tam and A. E. Hosoi, Phys Rev. Lett. **98**, 068105 (2007); J. E. Avron and O. Raz, New J. Phys. **10**, 063016 (2008).

[7] K. E. Machin, J. Exp. Biol **35**, 796 (1958).

[8] S. Camalet, F. Jülicher, and J. Prost, Physical Review Letters **82**, 1590 (199); S. Gueron and K. Levit-Gurevich, Proc. Roy. Soc. B **268**, 599 (2001); E. A. Gaffney, H. Gadelha, D. J. Smith, J. R. Blake, and J. C. Kirkman-Brown, Annu. Rev. Fluid Mech. **43**, 501 (2011).

[9] C. H.Wiggins and R. E. Goldstein, Physical Review Letters **80**, 3879 (1998); E. Lauga, Physical Review E **75**, 041916 (2007).

[10] C. J. Brokaw, Science **178**, 455 (1972).

[11] C. Fang-Yen, M. Wyart, J. Xiea, R. Kawaia, T. Kodgere, S. Chena, Q. Wena, and A. D. T. Samuel, Proc. Natl. Acad. Sci. **107**, 20323 (2010).

[12] J. Gray and G. J. Hancock, J. Exp. Biol. **32**, 802 (1955); R. G. Cox, J. Fluid Mech. **44**, 791 (1970).

[13] J. Guckenheimer and P. Holmes, *Nonlinear Oscillations, Dynamical Systems, and Bifurcations of Vector Fields* (Springer-Verlag, New York, 1983).

[14] M. B. Sevryuk, Lecture Notes in Mathematics **1211** (1986); J. S. W. Lamb and J. A. G. Roberts, Physica D **112**, 1 (1998).

[15] Y. Or, Phys. Rev. E **82**, 065302(R) (2010); Y. Or, S. Zhang, and R. M. Murray, SIAM Journal of Applied Dynamical Systems **10**, 1013 (2011).

[16] G. J. Elfring and E. Lauga, Phys Rev. Lett. **103**, 088101 (2009); G. J. Elfring and E. Lauga, J. Fluid Mech. **674**, 163 (2011).

[17] E. Passov and Y. Or, Submitted, available online at www.technion.ac.il/~izi/publications.htm.

[18] A supplementary document with more technical details is submitted along with the manuscript via EPAPS